Optics Letters

"Hot-wire" microfluidic flowmeter based on a microfiber coupler

Shao-cheng Yan, Zeng-yong Liu, Cheng Li, Shi-jun Ge, Fei Xu,* and Yan-qing Lu

National Laboratory of Solid State Microstructures and College of Engineering and Applied Sciences, Nanjing University, Nanjing 210093, China
**Corresponding author: feixu@nju.edu.cn*

Received 13 September 2016; revised 15 November 2016; accepted 16 November 2016; posted 16 November 2016 (Doc. ID 275667); published 6 December 2016

Using an optical microfiber coupler (MC), we present a microfluidic platform for strong direct or indirect light-liquid interaction by wrapping a MC around a functionalized capillary. The light propagating in the MC and the liquid flowing in the capillary can be combined and divorced smoothly, keeping a long-distance interaction without the conflict of input and output coupling. Using this approach, we experimentally demonstrate a "hot-wire" microfluidic flowmeter based on a gold-integrated helical MC device. The microfluid inside the glass channel takes away the heat, then cools the MC and shifts the resonant wavelength. Due to the long-distance interaction and high temperature sensitivity, the proposed microfluidic flowmeter shows an ultrahigh flow rate sensitivity of 2.183 nm/(μl/s) at a flow rate of 1 μl/s. The minimum detectable change of the flow rate is around 9 nl/s at 1 μl/s.

OCIS codes: (060.1810) Buffers, couplers, routers, switches, and multiplexers; (060.2370) Fiber optics sensors; (060.2340) Fiber optics components.

https://doi.org/10.1364/OL.41.005680

Over the last several decades, microfluidics have been widely studied and developed in the field of chemical analysis and biological applications [1–3]. They play an important role in molecule detection, cell sorting, and counting. Microfluidic flow rate and flux are important indices of the applications.

Fiber-optic sensors have attracted much attention in recent years. Some novel fiber-optic structures such as fiber Bragg gratings (FBGs), Fabry–Perot interferometers (FPIs), and microfiber couplers (MCs) are utilized to sense the parameter variations, including ambient temperature, liquid refractive index, electric current, and magnetic field. Some "hot-wire" anemometers are proposed based on metallic coating such as silver film, combined with FPI and FBG [4–6]. Afterward, in the past two years, the fiber-optic microfluidic flowmeter is proposed based on FBG and "hot-wire" structure. They utilize the high-attenuation fiber where part of the incident power is absorbed by Co^{2+}-doped fiber core to generate heat and the output spectrum of FBG to recognize the flow rate variation [7,8]. The larger the flow rate is, the more heat microfluid takes away, and the more the spectrum shifts. Generally, the sensitivity of a fiber-optic "hot-wire" flowmeter seriously depends on the direct or indirect interaction length between the light and fluid and the temperature response of the fiber device, both of which are limited in these sensors.

In this work, we propose a kind of highly sensitive microfluidic flowmeter based on a lab-on-a-rod microfluidic platform. A so-called lab-on-a-rod device is formed by wrapping a microfiber or nanofiber with a strong evanescent field around a rod with several turns [9–11]. By tuning the pitch between turns and specializing the rod, a variety of functions can be achieved. Lab-on-a-rod microfluidic devices can be realized by employing a hollow rod or a thin-wall glass capillary to deliver liquid and interact with the evanescent field of the microfiber at the same time. Thanks to the unique geometry, the optical channels and liquid channels can be combined and divorced smoothly, without the conflict of input and output coupling. Moreover, not only a long interaction length between light and fluid but also a high temperature sensitivity can be easily achieved. Therefore, such a platform is attractive to highly sensitive "hot-wire" flowmeters. Here, we wrap a MC around a gold-coated glass capillary and then package the device by UV-curable adhesive which has a low refractive index to avoid environmental disturbance for long-term use. The evanescent field of the MC is absorbed by the gold film, then heat generates and warms the MC [12–14]. The microfluid flows through the glass capillary, takes away the heat, and in the meantime decreases the temperature of the MC. The output spectrum of the MC redshifts accompanied with varying temperature. The proposed microfluidic flowmeter is easy to fabricate, low-cost, well-packaged, and shows an ultrahigh sensitivity.

To fabricate the microfluidic flowmeter and realize the measurement of the flow rate, we use a MC fabricated by fusing and tapering two commercial single-mode fibers (SMF-28, Corning, USA) with the so-called flame brushing method. We strip the polymer coating around the single-mode fiber, parallel the two fibers, and fix them onto the motorized precision translation stages. A hydrogen-oxygen flame heats the two fibers. With stable, precise and computerized control, a MC forms. As seen from Fig. 1(a), the MC has three parts,

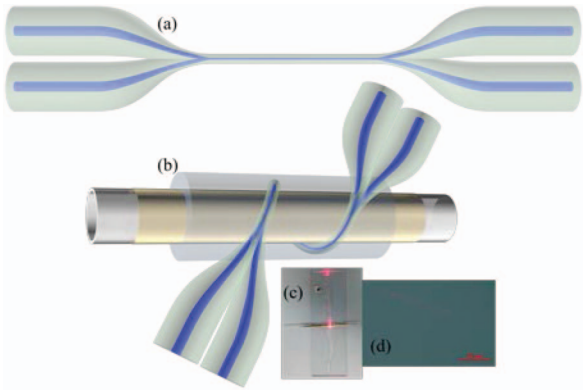

Fig. 1. Schematic diagram of (a) the MC and (b) the sensor. (c) Sensor packaged onto the glass slide. (d) Micrograph of the MC wrapping around the glass capillary and embedding in the UV-curable adhesive with the red laser injecting into the pigtail. The diameter of one of the MC is estimated to be 2–3 μm.

including one uniform waist region, two transition regions, and four pigtails. Light injects into one left pigtail, and exits from the right two pigtails. The output spectrum of the MC is shown in Fig. 2(a) with multiple interference peaks of a period of oscillating spectrum which can be explained by the interference of low-order symmetric and antisymmetric supermodes in the coupling region [15]. Every dip wavelength represents a characteristic wavelength of the MC, at which the power couples to another fiber at maximum efficiency. As for the slow modulation of the spectral envelope, it is because of the different coupling coefficients for x and y polarizations [16].

To fabricate the microfluidic flowmeter, we choose a glass capillary with the diameter approximately 1 mm and wall thickness approximately 120 μm as a microfluidic channel. With vacuum-coating technology, a 100-nanometer-thick gold film is coated around the capillary. After that, with the lab-on-a-rod technique, the MC is wrapped around the capillary with one

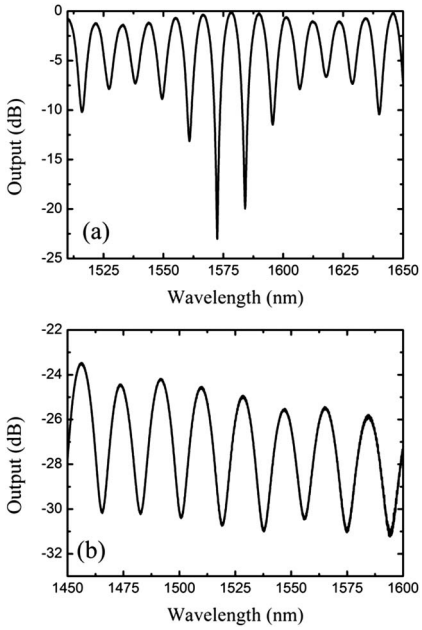

Fig. 2. Output spectra of (a) the MC and (b) the packaged sensor.

turn by a rotating stage. Finally, the sensing sections of the MC and the capillary are packaged with low-index polymer (LP). We choose a UV-curable adhesive (EFiRON UVF PC-375, Luvantix) with a refractive index of 1.38 as the LP. Then, the sensor forms as seen from Fig. 1(b). Figure 2(b) shows the output spectrum of the packaged sensor. The extinction ratio of the coupler decreases after packaging, which may result from the changing optical loss, the mismatch of the propagation constants, and the coupling coefficient between the two fibers. Besides, the modulation of the spectral envelope almost disappears because one polarization is almost absorbed.

Due to the absorption of the evanescent field by gold film, heat is generated and temperature increases. When the microfluid flows through the channel, it takes away part of the heat and cools the MC. The heat loss can be expressed as [17]

$$P_{\text{input}} \cdot a_{Au} \cdot \varphi = (A + B \cdot v^n) \cdot \Delta T, \tag{1}$$

where P_{input} is the incident power, a_{Au} is absorption efficiency of the gold film, φ is heat-transfer efficiency from the gold film to the inner wall of the glass capillary, v is the flow rate, A, B, and n are empirical calibration constants for the specific sensing channel and material of the microfluid, and ΔT is the temperature variation.

When the temperature decreases, the characteristic wavelength of the MC shifts according to the formula:

$$\Delta\lambda = k \cdot \Delta T \cdot \lambda_0, \tag{2}$$

where k is the temperature coefficient including the thermo-optic (TO) coefficient and thermal-expansion (TE) coefficient of the optical MC and the UV-curable adhesive. λ_0 is the characteristic wavelength.

By combining Eqs. (1) and (2), the relation between characteristic wavelength and the microfluidic flow rate is as follows:

$$\lambda = \left(1 + \frac{k \cdot P_{\text{input}} \cdot a_{Au} \cdot \varphi}{A + B \cdot v^n}\right) \cdot \lambda_0. \tag{3}$$

In the experiment, the broadband amplified spontaneous emission (ASE) source (1525 ~ 1565 nm, ASE3710-23, Connet), which serves as both pump and signal light, is injected into one of the pigtails of the MC. And the optical spectrum analyzer (OSA, YOKOGAWA AQ6370C) is used to receive the power from the opposite pigtail and records the output spectra.

Figure 3(a) shows the relation between the characteristic wavelength and the incident power from the ASE. Increasing the incident power raises the temperature and blueshifts the output spectrum of the MC. Figure 3(b) shows the relation between characteristic wavelength and the ambient temperature variation. A heater is used to heat the device up simulating the variation of ambient temperature, and the temperature is recorded with a thermocouple in real time. The heater can produce a very high temperature response of approximately 1.2 nm/°C. Such a microfiber device embedded in a low index polymer can work well in a wider ambient temperature range [10,18]. Combining Figs. 3(a) and 3(b), the temperature response caused by the absorption of the incident power is approximately 0.075°C/mW.

The microfluid is injected into the glass capillary with help from the syringe pump (SPLab01, Shenchen). We set the incident power to 197, 150, and 100 mW. Similarly, the larger

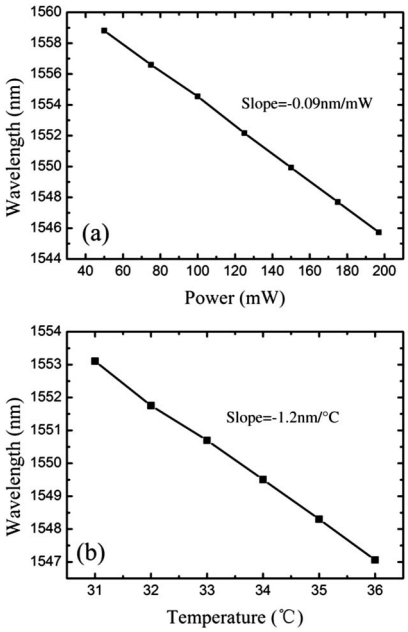

Fig. 3. Relations between characteristic wavelength and (a) the incident power from ASE and (b) ambient temperature variation.

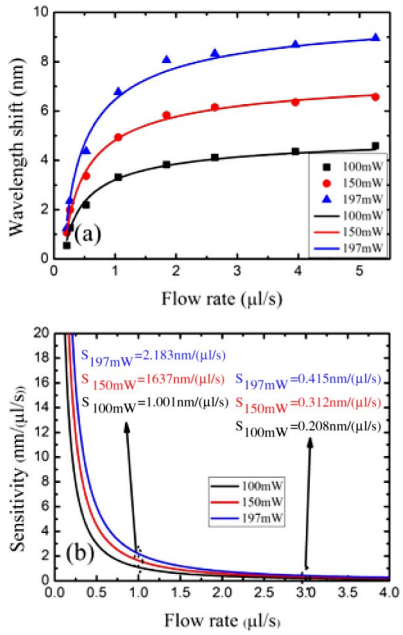

Fig. 4. (a) The output spectra of the MC shift with different microfluidic flow rates under different incident power values of 100, 150, and 197 mW. The curves are calculated fitting results based on Eq. (3). (b) The sensitivity (the first derivative of the calculated curves) is a function of different microfluidic flow rates.

the microfluidic flow rate is, the larger are the characteristic wavelength shifts, as seen in Fig. 4(a). The wavelength shift varies by the same proportion as the incident power. The curves are fitting results according to Eq. (3). Based on the fitting, the parameter n is estimated to be 0.6. When the flow rate increases to 3 μl/s, almost all the heat is taken away, and the wavelength shifts reach a saturation value. However, the saturation point could drift to a larger one by the following methods: increasing the incident power and the absorption of the evanescent field, using a thinner capillary channel, increasing the interaction length, tuning the absorption wavelength, and monitoring of multiple resonance peaks.

To estimate the sensitivity at one specific flow rate, the first derivative of the calculated curves in Fig. 4(a) is analyzed, as observed in Fig. 4(b). When the flow rate is larger than 1.5 μl/s, the calculated curves are almost linear. At $v = 3$ μl/s, the sensitivities are approximately 0.208, 0.312, and 0.415 nm/(μl/s), when the incident power is set to 100, 150, and 197 mW. While at $v = 1$ μl/s, the sensitivities are approximately 1.092, 1.637, and 2.183 nm/(μl/s), when the incident power is also set to 100, 150, and 197 mW. At $v = 1$ μl/s, there is almost one order of magnitude improvement in the sensitivity than for previous reports [7,8]. Because the resolution of the OSA is 0.02 nm, the minimum detectable change of the flow rate is approximately 48 nl/s at $v = 3$ μl/s and 9 nl/s at $v = 1$ μl/s when the incident power is 197 mW. It is ~16 nl/s at 1 μl/s with the incident power of 878 mW and the resolution of OSA of approximately 5 pm in a previous paper [7]. A smaller minimum detectable change of the flow rate could be acquired, if a larger pump power is incident and OSA with a smaller resolution is used. Besides, in the experiment, we only need to use one laser source because both the pump and the signal produce light.

In theory, we study the relation between the sensitivity and the diameter of one of the MC. The output power of the MC is described by $P = P_0 \sin^2(CL)$, where P_0 is the incident power, L is the coupling length, and C is the coupling coefficient. Besides, $C = (3\pi\lambda/32n_1a^2) \cdot (1/(1 + 1/V)^2)$, where λ is the incident wavelength, n_1 and n_0 are the refractive indices of the MC and the LP, and a is the diameter of one of the MC. And $V = [2\pi a/\lambda](n_1^2 - n_0^2)^{1/2}$. The characteristic wavelength of the MC occurs when $CL = m\pi$, where m is an integer. According to Eq. (2), the temperature sensitivity is related to the TO coefficient and TE coefficient of the optical MC and the UV-curable adhesive. So, the relation is described as [10,19]

$$\left(\frac{d\lambda}{dT}\right) = \left(\frac{d\lambda}{dT}\right)_{\text{TO,LP}} + \left(\frac{d\lambda}{dT}\right)_{\text{TO,MC}} + \left(\frac{d\lambda}{dT}\right)_{\text{TE,MC}} + \left(\frac{d\lambda}{dT}\right)_{\text{TE,LP}}$$

$$\left(\frac{d\lambda}{dT}\right)_{\text{TO,LP}} = \frac{d\lambda}{dn_0}\cdot\frac{dn_0}{dT} = \frac{8\pi^2a^2n_0}{\lambda}\cdot\frac{1}{V^2(V-1)}\cdot\sigma_{\text{LP}}$$

$$\left(\frac{d\lambda}{dT}\right)_{\text{TO,MC}} = \frac{d\lambda}{dn_1}\cdot\frac{dn_1}{dT} = \frac{\lambda^2V^2(V+1) - 8\pi^2a^2n_1^2}{\lambda n_1V^2(V-1)}\cdot\sigma_{\text{MC}},$$

$$\left(\frac{d\lambda}{dT}\right)_{\text{TE,MC}} = a\frac{d\lambda}{da}\cdot\frac{da}{dT}\frac{1}{a} = a\alpha_{\text{MC}}\cdot\frac{d\lambda}{da} = \frac{2\lambda V}{V-1}\cdot\alpha_{\text{MC}}$$

$$\left(\frac{d\lambda}{dT}\right)_{\text{TE,LP}} = \gamma\lambda\alpha_{\text{LP}}, \tag{4}$$

where σ_{LP} and σ_{MC} are the TO coefficient of the low-index polymer and the MC, respectively. α_{LP} and α_{MC} are the TE coefficient of the low-index polymer and the MC, respectively. For silica, $\sigma_{\text{MC}} = 1.1 \times 10^{-5}$/°C, and $\alpha_{\text{MC}} = 5.5 \times 10^{-7}$/°C [10]. For the UV-curable adhesive, we can estimate the comprehensive effect of the TO and TE coefficient of UVF PC-375 is at a

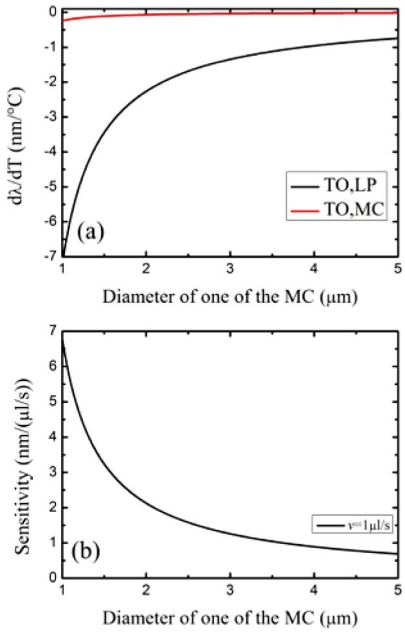

Fig. 5. (a) $d\lambda/dT$ at different diameters of one of the MC. (b) The relation between the sensitivity and the diameter of one of the MC at the specific microfluidic flow rate $v = 1$ μl/s, and the incident power is 100 mW.

magnitude of 10^{-4}/°C [18,20]. We induce $\gamma(0 < \gamma < 1)$ which represents the effective contribution on the MC from the thermal expansion of the UV-curable adhesive.

According to the calculation, the contributions from the thermal expansion effect are relatively small and can be neglected. Figure 5(a) shows the values of $d\lambda/dT$ contributed from the TO effects of the low-index polymer and MC at a different diameter of one of the MC. Combining Eqs. (2–4) and the estimated values of the empirical calibration constants (A, B, n) of the sensor, we can acquire the relation between the sensitivity and the diameter of one of the MC at one random specific microfluidic flow rate as seen in Fig. 5(b). According to Fig. 5(b), when the diameter of one of the MC is $2 \sim 3$ μm, the calculated sensitivity is $1 \sim 2$ nm/(μl/s) with the incident power of 100 mW and flow rate of 1 μl/s. The experimental result is 1.092 nm/(μl/s). As for the difference, it is attributed to the rough measurement of the diameter of the MC and the estimated TO coefficient of the UV-curable adhesive.

In the experiment, we also measure the dynamic response seen in Fig. 6. A tunable laser source with 30 mW is used with light injecting into one pigtail. The wavelength is chosen which falls at the falling edge of the output spectrum. The power meter is connected to the opposite pigtail. The microfluid cools the MC, and the output spectrum redshifts. The power rises at the chosen wavelength. The response time decreases from 153.8 to 14.8 s when the flow rate rises from 0.26 to 2.63 μl/s. The response time depends on $\Delta\lambda/v$. The higher the flow rate, the shorter the response time would be.

In conclusion, a new kind of microfluidic platform based on a MC lab-on-a-rod device is proposed, and we demonstrate its application on measurement of the microfluidic flow rate. The sensor is fabricated by wrapping the MC around the glass capillary which is coated by gold film in advance and packaging the MC with UV-curable adhesive for long-term use. The gold film

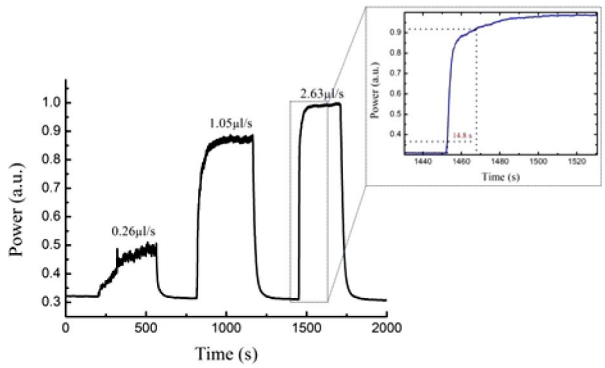

Fig. 6. Time responses under different microfluidic flow rates. The inset shows the response time is 14.8 s at 2.63 μl/s.

absorbs the evanescent field of the waist region, and heat is generated. Microfluid cools the MC, and the characteristic wavelength redshifts at a constant flow rate. In the experiment, only one laser source is used as both pump light and signal light. The sensor is easy to fabricate with a simple and reliable structure. Besides, it shows an ultra-high sensitivity, which is almost one order of magnitude higher than previous reports when the flow rate is 1 μl/s [7,8]. The minimum detectable change of the flow rate is 9 nl/s at $v = 1$ μl/s. It can be improved with a larger pump power and a smaller resolution OSA.

Funding. National Natural Science Foundation of China (NSFC) (61225026, 61535005, 61475069).

REFERENCES

1. G. M. Whitesides, Nature **442**, 368 (2006).
2. G. Velve-Casquillas, M. L. Berre, M. Piel, and P. T. Tran, Nano Today **5**, 28 (2010).
3. P. S. Dittrich and A. Manz, Nat. Rev. Drug Discov. **5**, 210 (2006).
4. X. Y. Dong, Y. Zhou, W. J. Zhou, J. Cheng, and Z. D. Su, IEEE Photon. J. **4**, 1381 (2012).
5. J. Cheng, W. J. Zhu, Z. W. Huang, and P. B. Hu, Sens. Actuators A **228**, 23 (2015).
6. X. H. Wang, X. Y. Dong, Y. Zhou, K. Ni, J. Cheng, and Z. M. Chen, IEEE Photon. Technol. Lett. **25**, 2458 (2013).
7. Z. Y. Liu, M. L. V. Tse, A. P. Zhang, and H. Y. Tam, Opt. Lett. **39**, 5877 (2014).
8. Y. Li, G. F. Yan, L. Zhang, and S. L. He, Opt. Express **23**, 9483 (2015).
9. M. Sumetsky, Opt. Express **12**, 2303 (2004).
10. Y. Chen, F. Xu, and Y. Q. Lu, Opt. Express **19**, 22923 (2011).
11. S. C. Yan, B. C. Zheng, J. H. Chen, F. Xu, and Y. Q. Lu, Appl. Phys. Lett. **107**, 053502 (2015).
12. P. B. Johnson and R. W. Christy, Phys. Rev. B **6**, 4370 (1972).
13. R. F. Oulton, V. J. Sorger, D. A. Genov, D. F. P. Pile, and X. Zhang, Nat. Photonics **2**, 496 (2008).
14. J. H. Chen, Y. Chen, W. Luo, J. L. Kou, F. Xu, and Y. Q. Lu, Opt. Express **22**, 17890 (2014).
15. Y. M. Jung, G. Brambilla, and D. J. Richardson, Opt. Express **17**, 5273 (2009).
16. F. P. Payne, C. D. Hussey, and M. S. Yataki, Electron. Lett. **21**, 561 (1985).
17. H. H. Bruun, *Hot-Wire Anemometry: Principles and Signal Analysis* (Oxford University, 1995).
18. X. Zeng, Y. Wu, C. L. Hou, J. Bai, and G. G. Yang, Opt. Commun. **282**, 3817 (2009).
19. L. F. Luo, S. L. Pu, J. L. Tang, X. L. Zeng, and M. Lahoubi, Appl. Phys. Lett. **106**, 193507 (2015).
20. P. F. Wang, M. Ding, G. S. Murugan, L. Bo, C. Y. Guan, Y. Semenova, Q. Wu, G. Farrell, and G. Brambilla, Opt. Lett. **39**, 5208 (2014).